Chapter Six

Modeling the Magnetization Process

6.1 Overview

Chapter 4 presents the magnetic properties of b-axis-oriented Dy, obtained by SQUID magnetometry. Chapter 5 provides an interpretation of these results, with calculations that support the measured magnetic phase diagrams. It establishes that the magnetoelastic Hamiltonian and magnetic domains both play important roles in the magnetization process; however, the clear separation of these two effects is not always easy. The research described in this chapter is an attempt to understand the contribution individual terms of the magnetoelastic Hamiltonian make to the ferromagnetic properties of b-axis-oriented Dy. Specifically, two calculations have been developed, the first a thermal equilibrium model and the second a model with thermal activation, to study magnetization in an applied field. These calculations provide significant insight into the physical origins of the magnetic ordering, including anisotropy, coercivity, and the wasp-waisted hysteresis loops.

This Chapter is organized in the following way. First, a brief review of contemporary magnetization calculations is given, with summaries of several early models, to place the present work in context and to identify the origins of the models presented in this Chapter. An overview of the magnetic energy landscapes then follows, so that such important features as appearance and disappearance of states are clearly identified. A thermal equilibrium model is described, along with a summary of results which identify the inadequacies of this model. The model which includes thermal

activation is presented next, followed by detailed results concerning domain wall pinning, temperature, and applied field. The conclusions of this research are presented at the end.

6.2 Brief Review of Magnetization Models

There are a large number of approaches to calculating magnetization, but most fall into two general categories: *micromagnetic models*, which self-consistantly determine the distribution of moments in a body [1],[2]; and *Néel-Brown-type models*, which calculate the time-dependence of magnetization using thermally-activated processes [3],[4]. The bulk of modern research concerns these two models. In addition, however, there are models based on specific integral or differential equations (such as the Preisach model, not discussed here [5],[6]), which tend to be of limited applicability; and *Stoner-Wohlfarth models*, which have enjoyed some success in qualitative predictions of hysteresis loop shapes [7]. The two models developed in this research are examples of Néel-Brown-type models which are applied to qualitatively modeling hysteresis loop shapes.

Micromagnetic Models

Micromagnetic modeling, which concerns the calculation of moments and domain behavior in an applied magnetic field, is a rapidly growing field. The equations governing the behavior of moments and magnetic domains were recognized as early as 1935 by Landau and Lifshitz [8], but recent technological interest in ultrasmall magnetic systems, together with advances in computational physics, has promoted a rapid development of detailed micromagnetic calculations of domain wall motion and hysteresis in an applied magnetic field.

The starting point for many current models of magnetization and domain growth is the Landau-Lifshitz-Gilbert (LLG) equation [1],

$$\frac{\partial \mathbf{M}}{\partial t} = g_G \mathbf{M} \times \mathbf{H} - \frac{a_G}{M} \mathbf{M} \times \frac{\partial \mathbf{M}}{\partial t} \tag{6.1}$$

where g_G and a_G are the Gilbert gyromagnetic and damping constants which describe the precession of moments in a time-varying field [2]. In fact, this is a phenomenological equation with a damping term that has not been derived from basic principles. Although not obvious, this can be re-written (e.g., Ref. [9]) in the small-damping limit as the magnetostatic Brown's equation

$$\mathbf{m} \times \left(C\nabla^2 \mathbf{m} + M_S \mathbf{H} - \frac{\partial w_a}{\partial \mathbf{m}} \right) = 0 \tag{6.2}$$

where w_a is an anisotropy energy density. Although mathematically complex, the essential physics expressed by Eq. (6.2) is that in equilibrium the torque everywhere is zero and the magnetization is parallel to an effective field,

$$\mathbf{H}_{\text{eff}} = \frac{C}{M_S}\nabla^2 \mathbf{m} + \mathbf{H} - \frac{1}{M_S}\frac{\partial w_a}{\partial \mathbf{m}} \tag{6.3}$$

The spatial distribution of magnetization can be determined self-consistantly using these equations, although sophisticated computational evaluation is required. Micromagnetic models have met with some success in systems for which magnetic domain structure has been measured. However, these are continuum models and, as such, they may not be applicable in highly anisotropic systems with very small domain walls.

Stoner-Wohlfarth Models

The best-known approach to modeling the magnetization of a single-domain ferromagnetic particle in an applied magnetic field is the Stoner-Wohlfarth model, developed in 1948 [7]. This model is based on the following ideas. The exchange energy of the moments in the domain is assumed to be strong enough to maintain the moments in a parallel configuration. The magnetic energy in an applied field is then calculated using shape and magnetocrystalline anisotropy, and Zeeman coupling to the field. As the field changes, the magnetization state follows the history-dependent local minimum, and hysteresis occurs because the energy expressions are multivalued. This simple model has met with considerable success, particularly in qualitatively predicting hysteresis in systems with

strong anisotropy. Recently, a SW model been developed by Huth and Flynn to study transition-metal rare-earth thin films [10].

A limitation of the Stoner-Wohlfarth model is that it follows the local energy minimum as the magnetic field changes, and it therefore ignores dissipation and thermal fluctuations between states of lowest energy. These temperature-dependent effects were first introduced by Néel and further developed by Brown, who assumed a thermal distribution of moments which could make transitions between states [11]. This led to a Fokker-Planck description of the probability density of orientations [12]. In the original work, this model was applied primarily provide a theoretical foundation for transition rates, but related Néel-Brown-type models (not necessarily involving Fokker-Planck equations) have since been applied to treat many magnetic phenomena, most notably time-dependent effects such as magnetic viscosity [13].

Present Research

This Chapter presents two models of the way the Hamiltonian enters into the magnetization process. They are essentially Néel-Brown-type models which involve thermal activation, but these are used to qualitatively understand hysteresis loop shapes. The first, which is termed here the thermal equilibrium model, is oversimplified but it nevertheless provides a useful description of the modeling procedure and clearly identifies specific physical characteristics to be improved. The second model, called the thermal activation model, was developed specifically to overcome the limitations of the thermal equilibrium model. The magnetic energy landscapes are first introduced, and then the models and the results of these calculations are described.

6.3 Energy Landscapes

A simplified model of the magnetization process requires that the stable states for a rare earth moment and their evolution in an applied field be calculated. These “energy landscapes” are to be described by the Hamiltonian presented in Chapter 1, which is the

sum of magnetocrystalline, magnetoelastic, and shape anisotropies, and Zeeman coupling to the applied field,

$$H = H_{\mathrm{CF}} + H_{ME} + H_{\mathrm{S}} + H_{\mathrm{Z}} \tag{6.4}$$

Some important assumptions made throughout this Chapter are first documented.

Uniaxial anisotropy. Since uniaxial anisotropy is strong ($K_2 >> K_6^6$) for Dy, in what follows all moments are assumed locked to the basal plane; only the f-dependence of the interactions is included, with $q = p/2$. For Dy this means that applied field will be assumed to lie in the basal plane. This is valid for xy-model rare earths such as Dy, Tb, and Ho, in which strong magnetocrystalline anisotropy restricts the moments to lie in the plane. For rare earths which order in three dimensions, such as Er, the energy landscapes are more complicated and it is not yet clear if these models can provide an accurate description of ordering.

No exchange coupling. The system is assumed ferromagnetic. The magnetoelastic Hamiltonian (Eq. (6.4)) does not include the exchange interaction which, for a single ferromagnetic domain, appears as a constant energy offset. This necessarily excludes rare earths such as Er, in which the ferromagnetic state involves exchange coupling.

Crystal lattice and strain. The crystal lattice is assumed constrained by chosen epitaxial strain and clamping. The system is always ferromagnetic, and the lattice parameters are fixed. Therefore the purely elastic interaction H_E is ignored. The possibility of magnetostriction from the growth and coalescence of ferromagnetic domains is not considered. Experimental measurements of this possible effect, now in progress by C. Durfee, will be welcome.

No interdomain effects. In real systems dipole coupling between domains is important, but this can be handled adequately only in a micromagnetic (i.e., LLG) framework.

Energy Landscapes

Based on the magnetoelastic Hamiltonian, the free energy depends on the direction of the moments and the strength and direction of the applied field. The “energy landscapes”

presented in Chapter 5 showed that magnetoelastic coupling and shape anisotropy generate a unidirectional in-plane easy axis for stretched Dy and, similarly, two out-of-plane easy axes for compressed Dy.

Now the evolution of these energy landscapes with applied field is considered. An example which highlights important features is presented. First, the free energy for clamped, unstrained Dy is shown in Figures 6.1, for the field applied along the in-plane a-axis. At zero applied field there a number of energy minima (which occur at polar angles f_i). These are separated by energy barriers so that, for a moment located in these states, additional energy is required for rotation into a different direction. As the magnetic field changes, the location and energy of the states f_i both change. This is a consequence of the Zeeman interaction which tends favors parallel alignment of the moments with the field. A second feature is that states may spontaneously appear or disappear, due to compensation of magnetic anisotropy by Zeeman coupling. Eventually, in strong enough fields, the Zeeman coupling overcompensates the intrinsic six-fold anisotropy and this eventually forces a disappearance of all non-parallel states.

The location of the stable states is easily determined. They are located by angles which minimize the free energy of Eq. (6.4), computed via the equilibrium condition

$$\left.\frac{df}{df}\right|_{f_i} = 0 \tag{6.5}$$

This is a transcendental equation but it is readily solved using a computational approach. The location of the stable states under an applied field is presented as Figure 6.2, for clamped, unstrained Dy.

The energy of these states is now addressed, with a view to their probability of occupation. For specified epitaxial strain and clamping, the state locations $f_i(H)$ are first calculated by Eq. (6.5), and these are then used to determine the energies, $E_i = f(f_i, H)$. The field-dependence of the energy of each state is presented in Figure 6.3. The energy of states parallel to or closely-aligned with the applied magnetic field decreases with increasing field, as expected. The state for $f_i = p$ (or more generally, states aligned against

the field direction) is clearly unfavored, as shown by an increasing free energy for this direction.

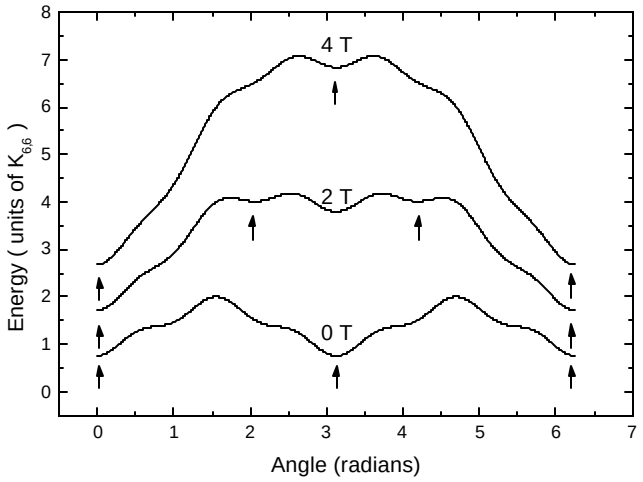

Figure 6.1: The free energy of a magnetic moment in clamped, unstrained Dy. The hexagonal symmetry is broken by shape anisotropy. The equilibrium locations are indicated.

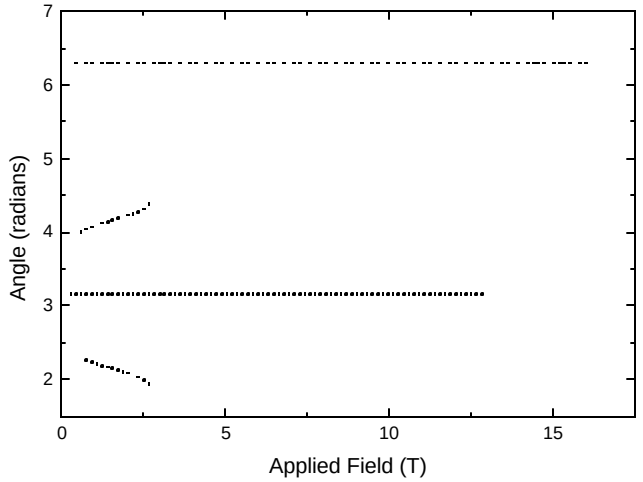

Figure 6.2. The evolution of stable states (free energy minima) as the applied magnetic field is increased. States may appear and disappear, but eventually (~8 T) the applied field forces alignment.

In summary the magnetoelastic Hamiltonian has well-defined energy states. As the applied magnetic field is increased the energy landscape evolves and hence the number of stable states, their location f_i and their free energy $E_i = f(f_i, H)$ also evolves. It is natural to inquire whether a probability of occupation can be associated with each state, and how transitions between these states can occur as the applied field is changed. The simplest model of this process is presented next.

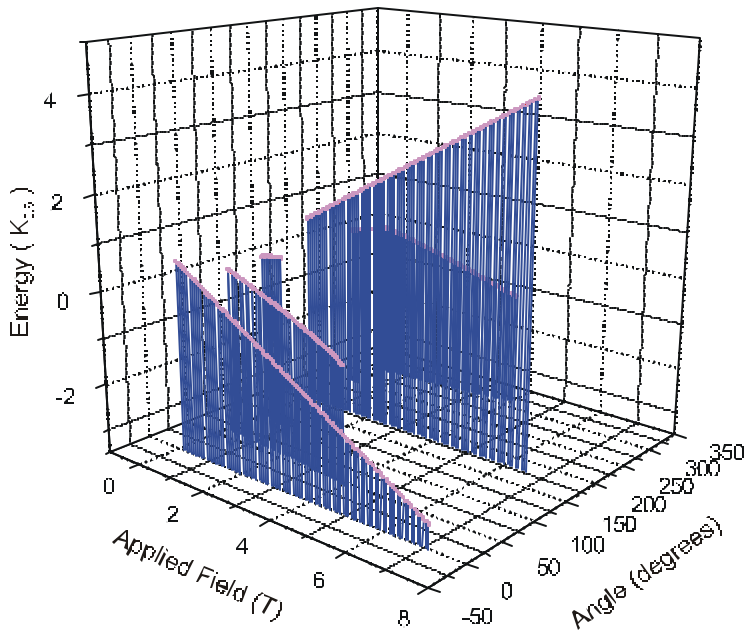

Figure 6.3. The free energy of the stable states in compressed Dy. The states along the field direction decrease in energy with increasing field, as expected.

6.4 Thermal Equilibrium Model

The simplest model of the magnetization process, governed entirely by the magnetoelastic Hamiltonian, assumes that the collection of states is occupied in thermodynamic equilibrium for all applied fields. Specifically, the magnetization profile is obtained by assuming each equilibrium state f_i of energy E_i contains a population of moments P_i which is proportional to the Maxwell-Boltzmann factor,

$$P_i = \exp(-E_i / k_B T) / Z \tag{6.6}$$

where the partition function

$$Z = \sum_i \exp(-E_i / k_B T) \tag{6.7}$$

ensures proper normalization of states. Interestingly, this is identical to the problem of quadrupolar defect orientations in an elastic stress field, discussed by Flynn [14]. Strictly, the Gibb's free energy (*G=E-TS*) must appear in the numerator of Eq. (6.7). Since the present system contains only a small number of states (at most, 6), the entropic contribution to the free energy is ignored.

The net magnetization described by this model is then the projection of the moments in the field direction,

$$\begin{aligned} M &= \sum_i \mathbf{m}_i \cdot \mathbf{H} \,/\, |\mathbf{H}| \\ &= m \sum_i \exp(-E_i \,/\, k_B T) \cos(f_i - f_0) \,/\, Z \end{aligned} \tag{6.8}$$

where each moment has magnetic dipole strength m, and the angles f_i are defined with respect to the applied field direction, f_0.

Finally, the modeling procedure can be written as the following sequence of steps, also shown in Figure 6.4:

1. Select the initial magnetic field *H*.
2. Compute the quantities $f_i(H)$, $E_i(H)$, $P_i(H)$.
3. Use these quantities to compute the net magnetization *M*.
4. Change the magnetic field to $H+\Delta H$ and repeat this process.

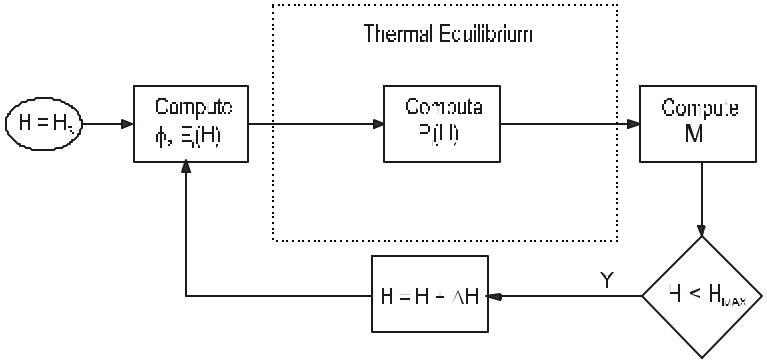

Figure 6.4. Flowchart of the thermal equilibrium model of magnetization.

Results and Inadequacies

The result of this model are magnetization curves, *M(H)*, shown as Figure 6.5. Only the data for positive fields are shown, but these are equivalent to magnetization for negative fields (*M(H)=-M(-H)*) by symmetry. There are two important aspects of these magnetization profiles. 1) *Hysteresis.* The system is always in equilibrium, so that hysteresis, coercive fields and remanent magnetization are not observed (i.e., there is no "history" in the magnetization process). Real magnetization curves show significant hysteretic effects, so this is a shortcoming of this model. 2) *Abrupt kinks.* As new states appear or disappear, these induce a significant repopulation of existing states, in accordance with the overall partition function normalization. In general real magnetization data do not show such distinct changes in the slope of *M(H).*

A similar model which involves thermal activation across the energy barriers has been developed to overcome these deficiencies, and this is discussed next.

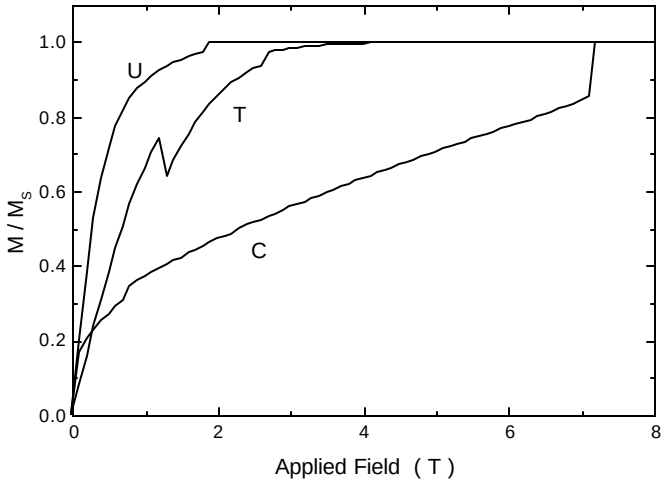

Figure 6.5. Magnetization curves calculated using the thermal equilibrium model, for unstrained (U), tensile (T), and compressively (C) strained b-axis-oriented Dy. Notice the unphysical, abrupt reduction or increase in magnetic moment, associated with the spontaneous disappearance or appearance of states. Since these states have free energies comparable with those of existing or persisting states, the sudden, non-negligible population of these states has a large effect on the net magnetization.

6.5 Thermal Activation Model

The thermal equilibrium model is a first step towards simulation of the magnetic ordering process using the magnetoelastic Hamiltonian, but this model had several unphysical difficulties. A model that includes thermal activation was developed to study path-dependent behavior. This Section is organized in the following way. First, the basic concepts of transition state theory are reviewed. This establishes the ideas of thermal activation with some rigor. Next, the thermal activation model is described so that the way deficiencies of the thermal equilibrium model are overcome is made clear. Subsequently, the model is applied to closely examine some experimental results, already presented in Chapter 4. The subsequent Sections apply the model to qualitatively examine some of the features of the hysteresis loops presented in Chapter 4. The emphasis is on what adjustments are needed (if any) to obtain agreement with experiment. Finally, the conclusions are summarized.

Transition State Theory

Obtaining the equations of motion for particles confined to an energy landscape (reaction coordinate) has been studied by Van't Hoff, Arrhenius, Kramers and others since 1880. The general problem is known reaction-rate theory, and recently an authoritative review [15] was given by Hänngi et al. This Section presents the essential ideas, to place the thermal activation model into proper perspective and to show how extension or generalization of this model may be possible.

The "particles" (in the present case, a collection of coherent magnetic moments) are confined to the energy surface shown in Figure 6.6. There are metastables states at A and C, separated by energy barriers $E_B^{\pm}$, and escape from these occurs via forward and backward rates, $k^{\pm}$. If the system is assumed to be in contact with a heat reservoir, then quantities such as dissipation and entropy may be rigorously included (in the present model, these are ignored). The scope of reaction-rate theories are extremely broad, and they encompass classical motion, tunneling between states, and admixtures of these

processes. An important class of reaction-rate theories, known as transition state theories (TST), concerns the passage of particles through a transition state without return [15]. Before describing the thermal activation model, two central TST results will be given. These concern the separation of time scales, and the Master equation which governs the time-evolution of the occupation probabilities.

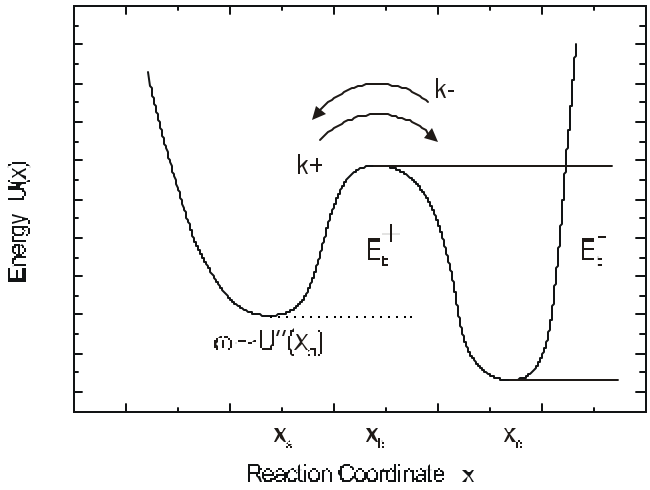

Figure 6.6. A potential U(x) with two metastable states, to illustrate the transition-state theory.

Separation of time scales. As discussed in Ref. [15], the time scale of escape of a particle across a barrier depends on the size of the thermal fluctuations (with energy $E_{noise} = k_B T$), and transitions will be infrequent when

$$\frac{E_{noise}}{E_b^{\pm}} << 1 \tag{6.9}$$

According to TST, the time scale which describes motion within the state is related to the curvature of the energy surface U,

$$t_s \sim M^{1/2}\left[\frac{d^2U(x=a)}{dx^2}\right]^{-1/2} \tag{6.10}$$

where M is the mass of the particle. Thus, the escape time is well-separated from this when

$$t_e \sim t_s \exp(E_b^{\pm} / E_{noise}) >> t_s \tag{6.11}$$

This condition is fulfilled in the present thermal activation model; that is, the model concerns the response of the magnetization to a slowly changing applied field, not the time-dependence of magnetization at short times; magnetic attempt frequences are typically $10^9 - 10^{10}$ sec^{-1} [13]. The time coordinate is then an effective variable to generate hysteresis, rather than for rigorous calculation of time-dependent magnetization measurements.

Master equation. In the thermal equilibrium model it is assumed that moments are free to occupy new states as the energy landscape evolves, ignoring energy barriers which separate states. For slow changes of magnetic field, one can consider instead a model in which the population of any state f_i may be decreased or increased by transitions to or from adjacent states $f_{i\pm1}$. In such cases, the Master equation provides a well-developed prescription for studying the *approach* of such a system to equilibrium [16].

The probability P_r that a state will be occupied depends on the probability p_{rs} that moments can rotate into other states, as well as the probability that moments can rotate into this state from other states, p_{sr}. The time dependence of P_r is then described by the "master equation" [16],

$$\frac{dP_r}{dt} = \sum_s P_s p_{sr} - \sum_s P_r p_{rs} \tag{6.12}$$

Since time enters this equation linearly in the first derivative, the master equation does not remain invariant as the sign is reversed from t to $-t$. In this way, this equation describes the irreversible behavior of the system [16].

The Thermal Activation Model

The approach taken in this Section is to solve Eq. (6.12) numerically. Since the model describes the rotation of moments, only transitions between adjacent states will be allowed. The transition probabilities must be specified. Surrounding a state f_i there are energy barriers $B_{i,i+1}$ and $B_{i,i-1}$ between the adjacent states f_{i+1} and f_{i-1}, respectively

[17]. Let the probability for a moment to rotate into an adjacent state depend on thermal activation across the separating energy barrier, so that

$$p_{i,i\pm1} = \exp(-B_{i,i\pm1} / k_B T) / Z \tag{6.13}$$

Since the master equation is a system of coupled first order ordinary differential equations, Euler's method may be used for a numerical solution [18]. This is a step-wise solution which involves rewriting Eq. (6.12) as the difference expression

$$P_i^{(1)} = P_i^{(0)} + \left(P_i^{(0)} p_{\,i,i+1} + P_i^{(0)} p_{\,i,i-1} - P_{i+1}^{(0)} p_{\,i+1,i} - P_{i-1}^{(0)} p_{\,i-1,i} \right) \tag{6.14}$$

This must be applied in succession to all states, and periodic boundary conditions are used since the process describes rotation. In the limit of $P_i^{(N)}$ with large N, equilibrium is obtained. The thermal activation model is concerned with a qualitative interpretation of hysteretic effects, however, not the equilibrium solution and (more importantly) not with rigorous time-dependent results. Thus N is used as an adjustable parameter of the model, in order to vary the extent of magnetic hysteresis.

This model is unlike the thermal equilibrium model, in which the probability of occupation of a state could be computed at any time, without regard to the previous occupation of that state. In the present model, the occupation of a state now depends on the history of that state as well as the history of adjacent states, and magnetic hysteresis is therefore an intrinsic property of this model.

Initial conditions. Since hysteresis is important, the initial conditions must be appropriately specified. In the calculation of a full hysteresis loop, it is sufficient to begin the loop at an applied field which saturates magnetization ($H = H_{\text{sat}}$). Hysteresis will develop naturally as the applied field is swept. The initial conditions for the calculation of an initial magnetization curve are less clear. In the real system, the magnetization after zero-field cooling is negligible, because a domain structure establishes to minimizes internal energy (dipole, demagnetization, etc.). In the model, the system is preconfigured using a Maxwell-Boltzmann distribution and, because of π-rotational symmetry, there is no initial magnetization at zero field. This is not a shortcoming, however. The intent of the

model is to gain semi-quantitative intuition into the magnetization behavior which would result if the system were purely governed by the magnetoelastic Hamiltonian, thus the initial conditions can therefore be adjusted as necessary.

Activation volume. For magnetic systems the attempt frequency ν is known to be $10^9 - 10^{10}$ s, so that the energy contribution of thermal activation to overcoming energy barriers is $E_{th} = k_B T \log(tn)$ [13]. The Zeeman energy H_Z and other energies are extremely large in comparison. This "problem" has long been recognized [19], and it is a universal feature of thermally-activated models of magnetization [20]. Related problems exist, for example, in the Stoner-Wohlfarth model [10], and in models of vortex excitations in superconductors [21]. The idea is that the energy scale is relevant to the volume in which the magnetization behaves coherently (called the activation volume, and defined by the magnetic coherence length) rather than the atomic volume of a single moment. In terms of Eq. (6.12), the eigenvalues and eigenstates of the interacting system must be obtainied and there is no a priori knowledge on which length scales the moments are correlated for any given eigenstate.

Different defintions of the activation volume have been used, and some recent work has tried to connect the results of modeling with experimental measurements of this quantity [22]. The present research focuses on the qualitative shapes of hysteresis loops, not the exact time dependence of magnetization. Thus the energies per unit cell of Dy are employed, and the temperature is used as an effective variable.

Finally, the modeling procedure can be written as the following sequence of steps, also shown in Figure 6.7:

1. Select the initial magnetic field *H*.

2a. Specify / compute the quantities $f_i(H), E_i(H), P_i^{(0)}(H)$.

2b. Calculate the new occupancies $P_i^{(1)}$.

2c. Repeat the occupancy calculation through to $P_i^{(j)}$, where $j < N$ represents the desired effective magnetic relaxation time

3. Use these quantities to compute the net magnetization *M*.

4. Change the magnetic field to $H+\Delta H$ and repeat this process.

The remainder of this Chapter discusses results of this model.

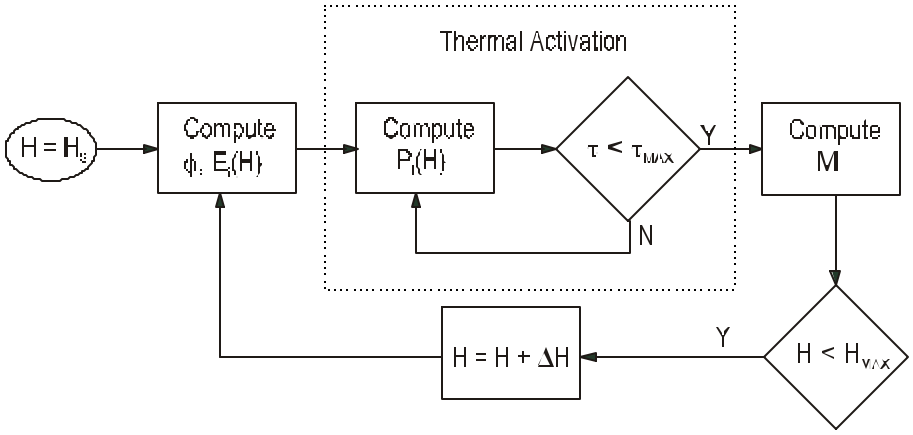

Figure 6.7. Flowchart of the thermal activation model.

Magnetization of Previously-Unmagnetized Samples

The calculated initial magnetization of compressed and stretched b-axis-oriented Dy are shown in Figure 6.8 which also contains, for convenience, the experimental result from Chapter 4. An interesting feature is that the calculated curve for compressed Dy shows an abrupt kink. Good agreement between calculated and observed kinks can be obtained simply by a slight reduction of the magnetoelastic constant from λ_2 = -0.0097 to λ_2 =-0.007. There is considerable spread in the measured (bulk) values of these coefficients and the coefficients for a thin film are likely to differ significantly from these, so is not a shortcoming. It is interesting that reasonable agreement can be obtained with a small readjustment of a single parameter.

The case of tensile strain is less encouraging. The data show a continuous and smooth approach to saturation, whereas the model predicts a negligible magnetization until a large switching field is encountered, at which point the magnetization abruptly saturates. This is not a failure of the thermal activation model; rather, it provides insight not readily available with other means. First, Chapter 4 showed that samples with tensile

strain are spontaneously ferromagnetic, with an easy axis parallel to the in-plane a-axis. The calculation appropriately reflects this easy axis by the sudden jump to saturation. Second, since the energy barriers are large, the calculation suggests an additional mechanism, one not included in the magnetoelastic Hamiltonian, reduces the large coercive field and permits domain growth in small applied fields. It is long known that edge domains in thin films cancel demagnetizing fields and that growth of these domains plays an important role in the initial magnetization [23]. The thermal activation model suggests the greater importance of these effects in films with tensile strain. This point will be further discussed below.

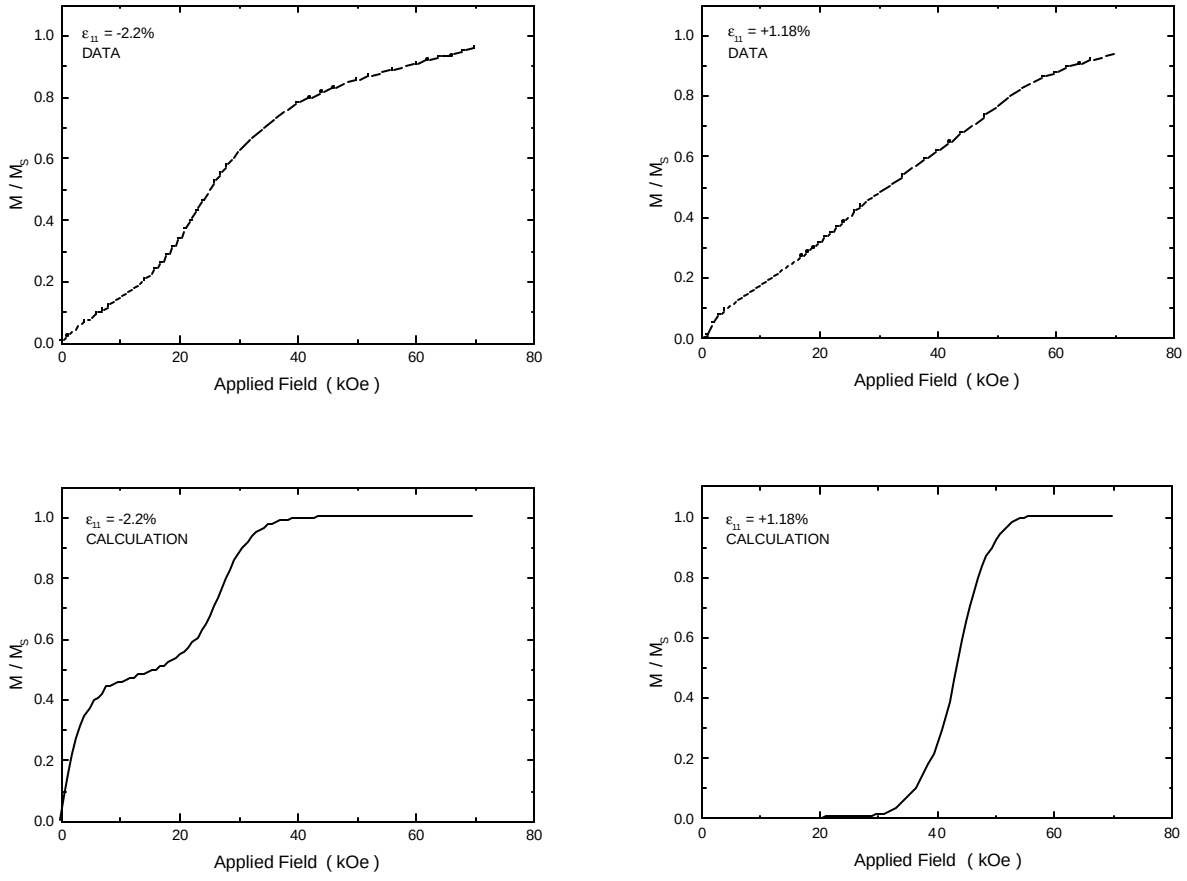

Figure 6.8. Measured (top) and calculated (bottom) initial magnetization curves for compressed (left) and stretched (right) Dy. For compressed Dy, the changes in slope at about 20 kOe and 40 kOe are reasonably well predicted by the calculation. For stretched Dy, there is reasonable agreement with the change in slope in 60 kOe, but the calculation clearly lacks a mechanism for spontaneous magnetization at low fields.

Hysteresis Loops

Hysteresis loops for b-axis-oriented Dy are calculated, using the parameters developed in the previous section. These are shown as Figure 6.9. The calculations exhibit two undesirable features. *Compressive strain.* The lack of hysteresis reflects the multiple states with small energy barriers, as shown in the polar diagram in Chapter 5. When the field is reversed new states develop and the energy barriers are such that these are easily populated in low applied fields. *Tensile strain.* The calculation predicts abrupt saturation with coercive fields larger than observed by experiments. Since domain wall pinning will increase the already-large coercive fields, the calculation suggests that a pinning mechanism will be an increasingly important contribution for increasing compressive strain. The effect of domain wall pinning is discussed next.

Domain Wall Pinning

Recall that Chapter 5 discusses that a domain wall pinning mechanism may be an increasingly important effect for increasing compressive strain. This is a mechanism whereby the system can achieve a state of lower free energy by coincidence of a domain wall with a defect, such as a dislocation, inclusion, or impurity [24]. Isotropic domain wall pinning can be incorporated into the thermal activation model by increasing the barrier heights which separate states, but leaving other parameters unchanged.

The calculation is modified in this way and two important results are immediately apparent; these are shown as Figure 6.10. First, keeping all other parameters fixed, the coercivity increases as the pinning potential increases. This behavior is expected, but it is reassuring to see that the most direct effect of pinning is on coercivity, rather than on other aspects of the calculation (such as saturation field, etc.). Second, for a pinning potential to produce reasonable coercivity, it must be roughly equivalent in magnitude to K_6^6, the basal plane anisotropy coefficient. This is reasonable, since the basal plane anisotropy establishes the baseline energy barrier for all states. Insofar as physical intuition regarding

the effect and magnitude of the pinning potential on the hysteresis loops would be otherwise difficult or impossible to develop, this again demonstrates the utility of these simple magnetization models.

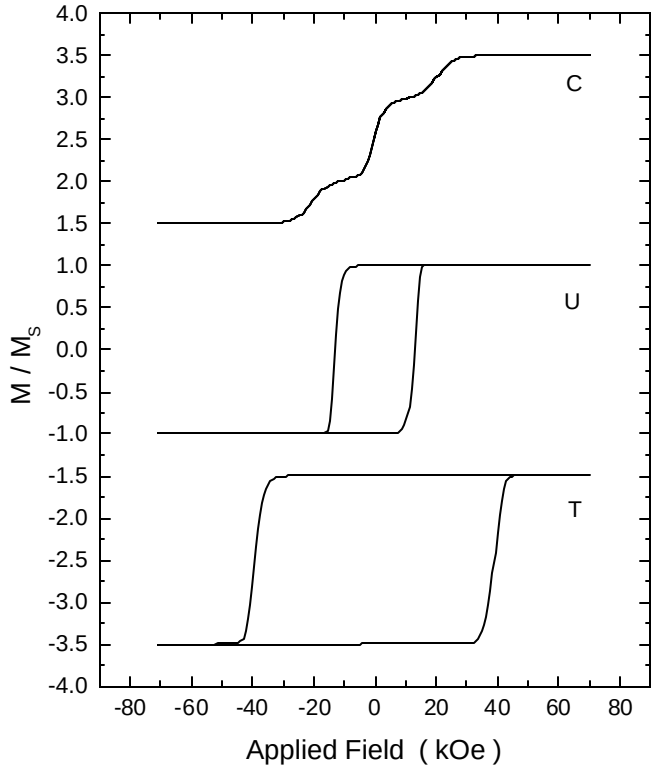

Figure 6.9. Calculated hysteresis loops, for compressive (C), unstrained (U) and tensile (T) b-axis-oriented Dy, using the parameters discussed in the text and neglecting any domain wall pinning mechanism.

Temperature Effects

The thermal activation model is used to study the effects of temperature on the hysteresis loops. It is clear that the energy barriers which separate states will become more surmountable with increasing temperature, so the coercive fields will decrease. However, the effect of temperature on the *shape* of the hysteresis loops is less clear.

The effect of temperature on the hysteresis loops for compressed and stretched Dy is shown in Figures 6.11 and 6.12. Two features are immediately apparent. First, the

coercive field is reduced with increasing temperature, reflecting the increasing ability for moments to surmount energy barriers by thermal activation. Second, with increasing temperature the hysteresis loops for compressed Dy become increasingly wasp-waisted, in general agreement with the experimental data in Chapter 4. This reflects the reversibility of magnetization at low fields and an increasing tendency towards irreversible population of states at higher fields.

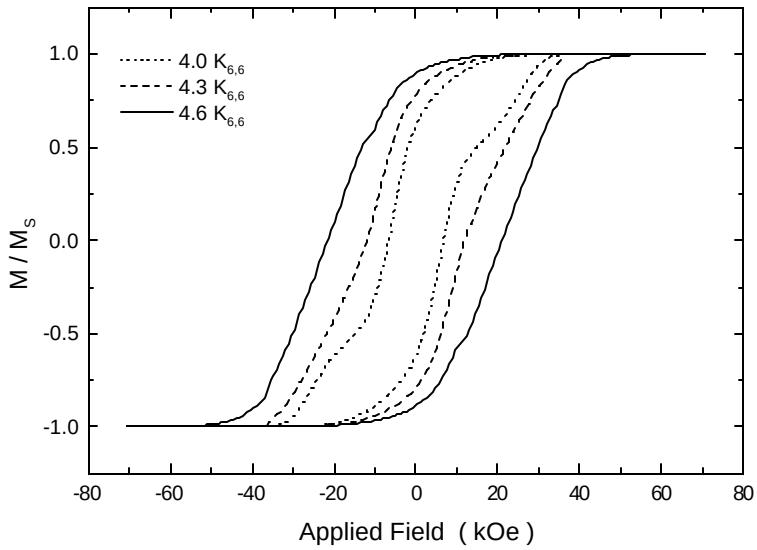

Figure 6.10. The effect of domain wall pinning in compressed Dy, for various values of the pinning potential. A pinning mechanism causes the hysteresis loops to open, giving rise to a coercive field which increases with increasing pinning.

Extension to Other Applied Field Directions

The magnetoelastic Hamiltonian for b-axis-oriented Dy shows the easy magnetization axes depend on strain. For tensile strain, there is a unidirectional easy axis along the in-plane a-axis. For compressive strain, the easy axes become canted towards the out-of-plane a-axes. Important corroborating evidence for this model was provided in Chapter 4 by a change in skewness of hysteresis loops collected with the applied field along the film-normal b-axis.

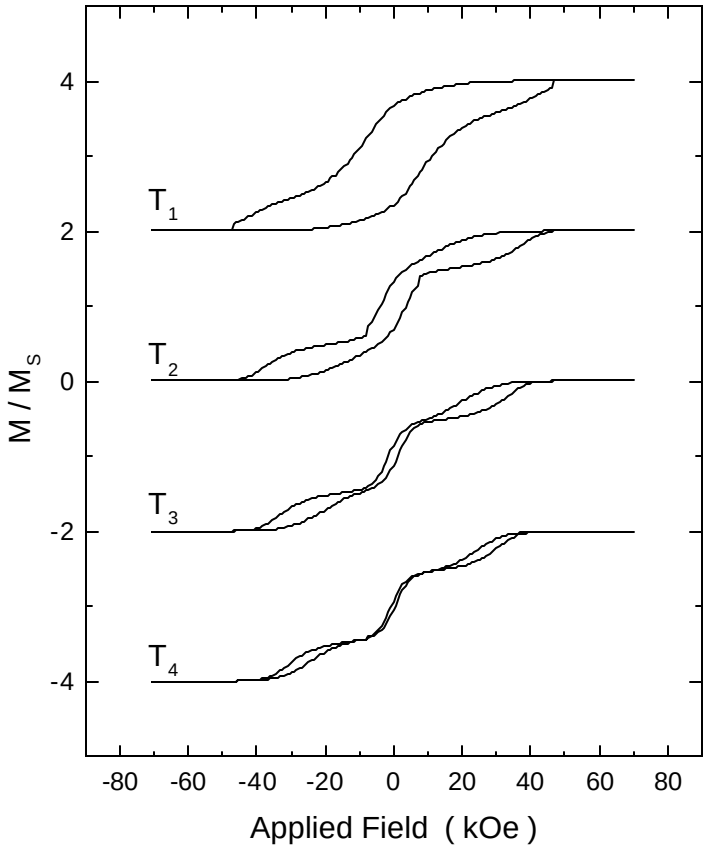

Figure 6.11. The effect of temperature on the hysteresis loops for compressed Dy. Increasing temperature gives rise to the narrow, wasp-waisted curves, exactly as in experimental data. Values here are 10 K through 14 K, but this is somewhat arbitrary according to the volume used for energy density conversion.

The magnetic anistropy is examined with the thermal activation model, by taking the applied field to be along the out-of-plane b-axis. Figure 6.13 presents calculations performed for a range of compressive and tensile strain. The calculation also shows that the out-of-plane b-axis becomes an increasingly-easy magnetization axis for increasing compressive strain, in agreement with the experimental results in Chapter 4.

Unfortunately, as discussed in the previous Section, restriction of this model to moments which lie in the basal plane precludes calculations of hysteresis loops with the applied field along the in-plane c-axis.

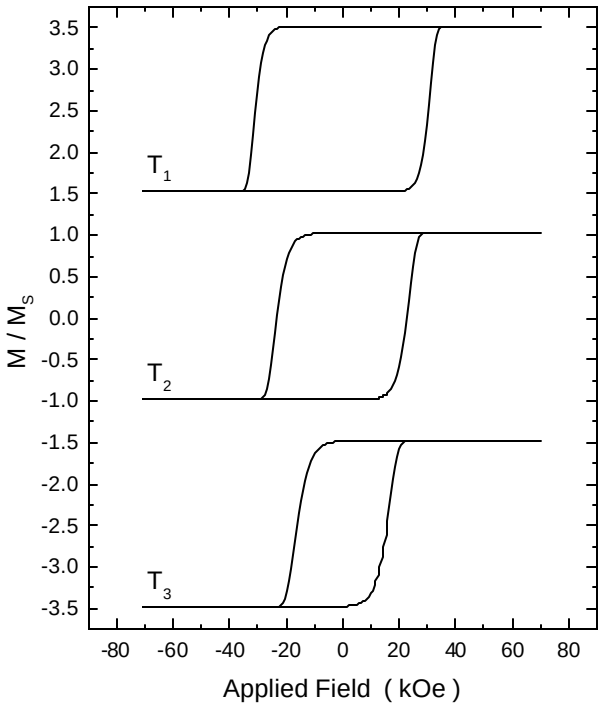

Figure 6.12. The effect of temperature on the hysteresis loops for stretched Dy. As the temperature is increased, barriers are more easily surmounted by thermal activation and the coercive field is subsequently reduced.

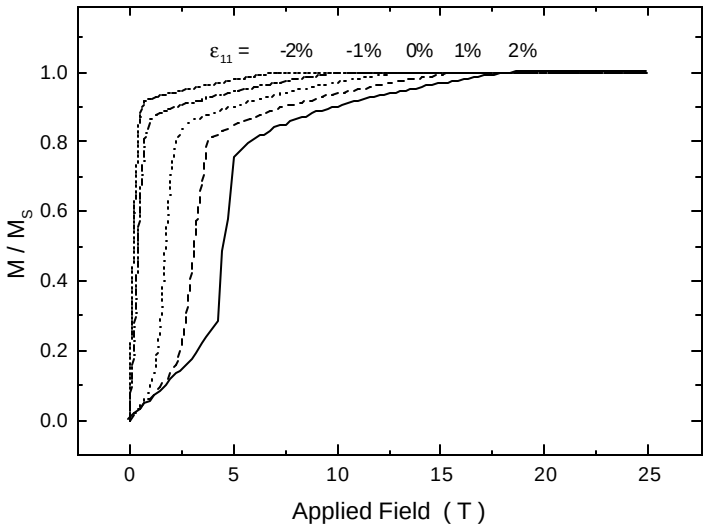

Figure 6.13. Calculated virgin curves for b-axis-oriented Dy with the applied field along the film-normal b-axis. Curves for a complete range of strain are provided, demonstrating that the film-normal b-axis becomes an increasingly-easy magnetization axis with increasing compressive strain, as predicted by the magnetoelastic Hamiltonian.

6.6 Summary

Magnetization in an applied magnetic field depends on the behavior of magnetic domains as well as the Hamiltonian which governs the moments. For the case of b-axis-oriented Dy, this complicated problem has been diagonalized to study the dependence of the magnetization on the Hamiltonian alone. Two models of magnetic ordering in b-axis-oriented Dy were presented: a thermal equilibrium model and a thermal activation model. The former assumes states are populated according to a Maxwell-Boltzmann distribution and therefore predicts no hysteresis effects. The latter assumes states are populated by transitions to and from adjacent states and therefore exhibits hysteresis. The important results of this work are derived from the thermal activation model, and these are summarized as follows:

1. The central result is verification that the magnetoelastic Hamiltonian causes hysteresis loops to "square up" as the strain is changed from compressive to tensile, reflecting the change in easy axis of magnetization from the canted, out-of-plane a-axis to a unidirectional in-plane a-axis.

2. Coercivity in compressed Dy was well-described by a domain wall pinning mechanism. The magnitude of the pinning potential is approximately that of the basal plane anisotropy, K_6^6.

3. The model predicts high coercivity for stretched Dy, resulting from deep in-plane magnetoelastic states. The coercivity decreases with increasing temperature. Since high coercive fields are not observed in real samples, this suggests an additional mechanism, possibly involving domains, lowers effective barrier heights in b-axis-oriented Dy.

4. Wasp-waisted hysteresis loops for compressed Dy result with increasing temperature, and these loops become square with increasing tensile strain. This agrees well with behavior observed in real samples. This may indicate the relative importance of the Hamiltonian over magnetic domain processes in the ferromagnetic ordering.

These models have been applied to varying applied magnetic fields (hysteresis loops), but they can be augmented to include possible changes in strain or other

parameters which may accompany magnetization. Work in progress by C. Durfee in this research group may elucidate the importance of these processes.

References

[1] T. L. Gilbert, J. M. Kelly, in *Proc. Conf. Mag. and Mag. Materials* (AIEE, Pittsburgh, 1955), 253-263.

[2] J. C. Mallinson, *IEEE Trans. Mag.* **23**, 2003-2004 (1987).

[3] The term "Néel-Brown model" is also used for magnetic transition state models in which the attempt frequency is constant.

[4] J. E. Wegrove, J. P. Meier, B. Doudin, J. P. Ansermet, W. Wernsdorfer, W. T. Coffey, Y. P. Kalmykov, J. L. Dejardin, *Europhys. Lett.* **38**, 329 (1997); W. Wernsdorfer, E. B. Orozco, K. Hasselbach, A. Benoit, B. Barbara, N. Demoncy, A. Louiseau, H. Pascard, D. Mailly, *Phys. Rev. Lett.* **78**, 1791-1794 (1997).

[5] See, for example, F. Preisach, *Z. Physik* **94**, 277 (1935); G. Bertotti, V. Basso, M. Pasquale, *IEEE Trans. Mag.* **30**, 1052-1057 (1994); G. Kadar, *J. App. Phys.* **61**, 4013-4015 (1987).

[6] D. C. Jiles, J. B. Thoelke, *IEEE Trans. Mag.* **25**, 3928-3930 (1989).

[7] E. C. Stoner, E. P. Wohlfarth, *Philos. Trans. Roy. Soc. London* **A240**, 599-642 (1948).

[8] L. Landau, E. Lifshitz, *Phys. Z. Sowj. Un.* **8**, 153-169 (1935).

[9] W. F. Brown, Jr., *Micromagnetics*, (Wiley, New York, 1963).

[10] M. Huth, C. P. Flynn, preprint.

[11] R. Street, J. C. Wooley, *Proc. Phys. Soc.* **62A**, 562 (1949); L. Néel, *J. Phys. Rad.* **11**, 65 (1950).

[12] W. F. Brown, Jr., *Phys. Rev.* **130**, 1677-1686 (1963).

[13] D. Givord, M. F. Rossignol, V. Villas-Boas, F. Cebollada, J. M. Gonzalez, in *Magnetic anisotropy and coercivity in rare earth/transition metal alloys, vol. 2*, F. Missel, ed. (World Scientific, Singapore, 1996).

[14] C. P. Flynn, *Point defects and diffusion* (Clarendon, Oxford, 1972).

[15] P. Hänggi, P. Talkner, *Rev. Mod. Phys.* **62**, 251 (1990).

[16] F. Reif, *Statistical and thermal physics* (McGraw-Hill, New York, 1965).

[17] The mean value theorem of calculus guarantees this.

[18] Burden, Faires, *Numical methods* (Addison-Wesley, New York, 1986).

[19] J. C. Barbier, *Ann. Phys. Paris* **9**, 84 (1954).

[20] See, for example, E. P. Wohlfarth, *J. Phys. F: Met. Phys.* L155-L159 (1984), and references therein.

[21] M. Huth, private communication.

[22] J. M. Gonzalez, R. R. Smirnov, J. Gonzalez, *IEEE Trans. Mag.* **33**, 4179-4181 (1997); A. Lyberatos, *J. App. Phys.* **75**, 5704 (1994).

[23] R. F. Soohoo, *Magnetic thin films* (Harper and Row, New York, 1965).

[24] I. Privorotskii, *Thermodynamic theory of domain structures* (Keter, Jerusalem, 1976).